

Optimization of single-cycle terahertz generation in LiNbO₃ for sub-50 femtosecond pump pulses

Maksim Kunitski,^{1,*} Martin Richter,¹ Mark D. Thomson,² Arno Vredenburg,¹ Jian Wu,³ Till Jahnke,¹ Markus Schöffler,¹ Horst Schmidt-Böcking,¹ Hartmut G. Roskos,² and Reinhard Dörner¹

¹*Institut für Kernphysik, Goethe Universität Frankfurt am Main, Max-von-Laue-Straße 1, 60438 Frankfurt am Main, Germany*

²*Physikalisches Institut, Goethe Universität Frankfurt am Main, Max-von-Laue-Straße 1, 60438 Frankfurt am Main, Germany*

³*State Key Laboratory of Precision Spectroscopy, East China Normal University, Shanghai 200062, China*
**kunitski@atom.uni-frankfurt.de*

Abstract: We compare different tilted-pulse-front pumping schemes for single-cycle THz generation in LiNbO₃ crystals both theoretically and experimentally in terms of conversion efficiency. The conventional setup with a single lens as an imaging element has been found to be highly inefficient in the case of sub-50 fs pump pulses, mainly due to the resulting chromatic aberrations. These aberrations are avoided in the proposed new setup, which employs two concave mirrors in a Keplerian telescope arrangement as the imaging sequence. This partially compensates spherical aberrations and results in a ca. six times higher conversion efficiency in the case of 35-fs optical pump pulse duration compared to the single-lens setup. A THz field strength of 60 kV/cm was obtained using 0.5 mJ pump pulses. The divergence of the THz beam has been found experimentally to depend on the pump imaging scheme employed.

©2013 Optical Society of America

OCIS codes: (300.6495) Spectroscopy, terahertz; (190.7110) Ultrafast nonlinear optics; (190.4400) Nonlinear optics, materials.

References and links

1. A. G. Davies, E. H. Linfield, and M. B. Johnston, "The development of terahertz sources and their applications," *Phys. Med. Biol.* **47**(21), 3679–3689 (2002).
2. M. C. Beard, G. M. Turner, and C. A. Schmuttenmaer, "Terahertz spectroscopy," *J. Phys. Chem. B* **106**(29), 7146–7159 (2002).
3. T. Feurer, N. S. Stoyanov, D. W. Ward, J. C. Vaughan, E. R. Statz, and K. A. Nelson, "Terahertz polaritonics," *Annu. Rev. Mater. Res.* **37**(1), 317–350 (2007).
4. H. G. Roskos, M. D. Thomson, M. Kreß, and T. Löffler, "Broadband THz emission from gas plasmas induced by femtosecond optical pulses: from fundamentals to applications," *Laser Photon. Rev.* **1**(4), 349–368 (2007).
5. M. C. Hoffmann and J. A. Fülöp, "Intense ultrashort terahertz pulses: generation and applications," *J. Phys. D Appl. Phys.* **44**(8), 083001 (2011).
6. D. You, R. R. Jones, P. H. Bucksbaum, and D. R. Dykaar, "Generation of high-power sub-single-cycle 500-fs electromagnetic pulses," *Opt. Lett.* **18**(4), 290–292 (1993).
7. H. Hamster, A. Sullivan, S. Gordon, W. White, and R. W. Falcone, "Subpicosecond, electromagnetic pulses from intense laser-plasma interaction," *Phys. Rev. Lett.* **71**(17), 2725–2728 (1993).
8. M. D. Thomson, V. Blank, and H. G. Roskos, "Terahertz white-light pulses from an air plasma photo-induced by incommensurate two-color optical fields," *Opt. Express* **18**(22), 23173–23182 (2010).
9. D. H. Auston, K. P. Cheung, J. A. Valdmanis, and D. A. Kleinman, "Cherenkov radiation from femtosecond optical pulses in electro-optic media," *Phys. Rev. Lett.* **53**(16), 1555–1558 (1984).
10. J. Hebling, G. Almási, I. Kozma, and J. Kuhl, "Velocity matching by pulse front tilting for large area THz-pulse generation," *Opt. Express* **10**(21), 1161–1166 (2002).
11. A. Stepanov, J. Kuhl, I. Kozma, E. Riedle, G. Almási, and J. Hebling, "Scaling up the energy of THz pulses created by optical rectification," *Opt. Express* **13**(15), 5762–5768 (2005).
12. A. Stepanov, S. Henin, Y. Petit, L. Bonacina, J. Kasparian, and J.-P. Wolf, "Mobile source of high-energy single-cycle terahertz pulses," *Appl. Phys. B* **101**(1-2), 11–14 (2010).

13. J. A. Fülöp, L. Pálfalvi, S. Klingebiel, G. Almási, F. Krausz, S. Karsch, and J. Hebling, "Generation of sub-mJ terahertz pulses by optical rectification," *Opt. Lett.* **37**(4), 557–559 (2012).
14. J. Hebling, A. G. Stepanov, G. Almási, B. Bartal, and J. Kuhl, "Tunable THz pulse generation by optical rectification of ultrashort laser pulses with tilted pulse fronts," *Appl. Phys. B.* **78**, 593–599 (2004).
15. J. Hebling, K.-L. Yeh, M. C. Hoffmann, B. Bartal, and K. A. Nelson, "Generation of high-power terahertz pulses by tilted-pulse-front excitation and their application possibilities," *J. Opt. Soc. Am. B* **25**(7), B6–B19 (2008).
16. L. Palfalvi, J. A. Fulop, G. Almasi, and J. Hebling, "Novel setups for extremely high power single-cycle terahertz pulse generation by optical rectification," *Appl. Phys. Lett.* **92**(17), 171107 (2008).
17. B. Schütte, U. Frühling, M. Wieland, A. Azima, and M. Drescher, "Electron wave packet sampling with laser-generated extreme ultraviolet and terahertz fields," *Opt. Express* **19**(20), 18833–18841 (2011).
18. A. G. Stepanov, L. Bonacina, S. V. Chekalin, and J.-P. Wolf, "Generation of 30 microJ single-cycle terahertz pulses at 100 Hz repetition rate by optical rectification," *Opt. Lett.* **33**(21), 2497–2499 (2008).
19. A. G. Stepanov, J. Hebling, and J. Kuhl, "Efficient generation of subpicosecond terahertz radiation by phase-matched optical rectification using ultrashort laser pulses with tilted pulse fronts," *Appl. Phys. Lett.* **83**(15), 3000–3002 (2003).
20. J. Fülöp, L. Pálfalvi, G. Almási, and J. Hebling, "High energy THz pulse generation by tilted pulse front excitation and its nonlinear optical applications," *J. Infrared Millim. Terahertz.* **32**(5), 553–561 (2011).
21. J.-C. Diels and W. Rudolph, *Ultrashort Laser Pulse Phenomena* (Elsevier, 2006).
22. J. A. Fülöp, L. Pálfalvi, G. Almási, and J. Hebling, "Design of high-energy terahertz sources based on optical rectification," *Opt. Express* **18**(12), 12311–12327 (2010).
23. J. A. Fülöp, L. Pálfalvi, M. C. Hoffmann, and J. Hebling, "Towards generation of mJ-level ultrashort THz pulses by optical rectification," *Opt. Express* **19**(16), 15090–15097 (2011).
24. G. Gallot and D. Grischkowsky, "Electro-optic detection of terahertz radiation," *J. Opt. Soc. Am. B* **16**(8), 1204–1212 (1999).
25. I. Z. Kozma, G. Almási, and J. Hebling, "Geometrical optical modeling of femtosecond setups having angular dispersion," *Appl. Phys. B.* **76**(3), 257–261 (2003).
26. R. Storn and K. Price, "Differential evolution – a simple and efficient heuristic for global optimization over continuous spaces," *J. Glob. Optim.* **11**(4), 341–359 (1997).
27. K. Nagashima and A. Kosuge, "Design of rectangular transmission gratings fabricated in LiNbO₃ for high-power terahertz-wave generation," *Jpn. J. Appl. Phys.* **49**(12), 122504 (2010).
28. Z. Ollmann, J. Hebling, and G. Almási, "Design of a contact grating setup for mJ-energy THz pulse generation by optical rectification," *Appl. Phys. B* **108**(4), 821–826 (2012).
29. K.-L. Yeh, M. C. Hoffmann, J. Hebling, and K. A. Nelson, "Generation of 10 μJ ultrashort terahertz pulses by optical rectification," *Appl. Phys. Lett.* **90**(17), 171121 (2007).
30. H. Hirori, A. Doi, F. Blanchard, and K. Tanaka, "Single-cycle terahertz pulses with amplitudes exceeding 1 MV/cm generated by optical rectification in LiNbO₃," *Appl. Phys. Lett.* **98**(9), 091106 (2011).
31. M. Nagai, E. Matsubara, and M. Ashida, "High-efficiency terahertz pulse generation via optical rectification by suppressing stimulated Raman scattering process," *Opt. Express* **20**(6), 6509–6514 (2012).
32. U. Frühling, M. Wieland, M. Gensch, T. Gebert, B. Schütte, M. Krikunova, R. Kalms, F. Budzyn, O. Grimm, J. Rossbach, E. Plönjes, and M. Drescher, "Single-shot terahertz-field-driven X-ray streak camera," *Nat. Photonics* **3**(9), 523–528 (2009).
33. I. Grguraš, A. R. Maier, C. Behrens, T. Mazza, T. J. Kelly, P. Radcliffe, S. Düsterer, A. K. Kazansky, N. M. Kabachnik, T. Tschentscher, J. T. Costello, M. Meyer, M. C. Hoffmann, H. Schlarb, and A. L. Cavalieri, "Ultrafast X-ray pulse characterization at free-electron lasers," *Nat. Photonics* **6**(12), 852–857 (2012).

1. Introduction

The applications of terahertz radiation in the range of 0.1–10 THz have expanded significantly in recent years and cover nowadays physics, biology, medicine, communication, material and environmental sciences [1–5]. For spectroscopy, the generation of coherent sub-picosecond single-cycle THz pulses by means of femtosecond near-IR pulses is highly attractive, since it allows one to perform broadband and time-resolved measurements using coherent time-domain sampling for detection. In recent years, efficient THz generation methods based on amplifier laser systems have reached fields in the kV/cm–MV/cm range and open the pathway to non-linear THz experiments while still remaining at a table-top scale.

The most widely used techniques for generation of THz pulses by employing femtosecond amplifier lasers are based on large-area photoconductive antennae [6], emission from a photoinduced gas plasma [4,7,8] and optical rectification (OR) in nonlinear crystals such as LiNbO₃ (LN) [9]. With regard to the latter approach, introduction of tilted-pulse-front pumping by Hebling et al. [10] in 2002 brought about a significant increase in efficiency for OR. The excellent energy scalability of this THz source [11] has allowed the generation of single-cycle THz pulses with an energy up to 50 μJ using 120 mJ (700 fs, 800 nm) pump

pulses [12]. Recently, 70 mJ laser pulses (1.3 ps, 1030 nm) have been employed for generation of 125- μ J THz pulses [13], which is the highest THz pulse energy reported to date among table-top sources.

Tilting the pulse front of the pump allows one to match its velocity to that of the THz radiation resulting in a far higher conversion efficiency. In the original proof-of-principle experiment, tilting of the pulse front was realized by diffracting the pump beam off a diffraction grating and subsequently imaging it onto the LN emitter crystal by means of a cylindrical lens [10]. The groove spacing of the grating, incidence angle and demagnification factor of the imaging system determine the resulting pulse front tilt, which in the case of LN for pump wavelengths around 800 nm should be about 62–64°. Since then several different imaging schemes have been proposed, based on a single spherical [14,15] or achromatic lens [16,17], a spherical concave mirror [18], a 1:1 Keplerian telescope [16] or a 2:1 Keplerian telescope made up of two achromatic lenses [19]. This variety of schemes is a result of attempts to find the ultimate imaging system where the detrimental effects of spherical and chromatic aberrations are minimized. These aberrations lead to pulse front distortions and spatial chirp, which, in turn, leads to a reduction of the overall conversion efficiency. Thus, Hebling and associates [16,20] proposed to omit the imaging optics completely, by bringing the crystal in contact with the grating. Realization of this approach is however technically challenging, as will be addressed later in this paper.

The imaging errors of an optical system become even more pronounced by going to shorter pump pulses. There are two reasons for this. Firstly, with broader optical pump spectra, it becomes more difficult to image all spectral components into the same spatial volume of the crystal because of chromatic aberrations. Secondly, the broader spectrum after diffracting off a grating acquires a higher divergence angle, and, as a result, requires larger apertures in the optical system. This, in turn, increases spherical aberrations during imaging, if the optical system consists of spherical components. Note that for both sources of aberration, it is the spectral width and geometric dimensions of the pump beam, but not the actual temporal length, which causes the imaging errors, and thus this issue cannot be solved by stretching the pump pulse in time.

There is another limitation for the THz yield in LN crystal when using very short pump pulses. Shorter pulses suffer from temporal broadening more rapidly while propagating in media with group velocity dispersion [21], and consequently lose their peak intensity faster than longer pulses. Since the THz conversion efficiency depends strongly on the laser intensity, the effective THz generation length in the crystal is smaller for shorter pulses, which causes a reduction of the THz yield. It was shown theoretically that the highest THz conversion efficiency is reached for 350-fs pump pulses [22]. Although even longer pulses result in a larger effective THz generation length, the increased THz absorption lowers the overall conversion efficiency [22]. Recent theoretical calculations predicted however that the highest THz efficiency may be achieved with a pump pulse duration of 500–600 fs [13,23].

Despite the two drawbacks described above, the use of a laser system with very short (i.e. sub-50-fs) pump pulses for THz generation in LN is sometimes necessary, when one requires such optical pulse durations in other parts of the experiment (e.g. for strong-field ionization or high-harmonics generation [17]). In this paper we aim to analyze the performance of the different imaging schemes for THz pulse generation based on optical rectification in a LN crystal specifically with such short optical pulses.

The paper is organized as follows. In the next section the experimental and simulation details are given. Then the different imaging schemes for THz generation are analyzed and compared in terms of the spatio-temporal imaging errors, as predicted from ray-tracing simulations. A comparison is made between the experimentally measured performance and these model predictions, and demonstrates which optical geometries are optimal for sub-50-fs optical pump pulses. In the conclusion section the main findings of the paper are summarized.

2. Experimental and simulations

2.1. Experimental

Two different femtosecond laser systems were utilized in the current work for performance comparison of THz sources with different imaging schemes. The first one is a multi-pass amplifier laser system (Dragon, KMLabs), which provides 35-fs pulses (FWHM) with 500- μ J pulse energy at a repetition rate of 8 KHz (center wavelength 780 nm, bandwidth 30 nm). The second laser is a 1-kHz regenerative amplifier laser system (Clark MXR CPA 2101), which generates \sim 150 fs pulses with a center wavelength of 780 nm, a bandwidth of 9 nm and an output energy of 500 μ J. The beams of both lasers were collimated to about 8 mm in diameter ($1/e^2$). In all tilted-pulse-front pumping schemes presented in this paper, a stoichiometric LiNbO₃ crystal (with a nominal 0.86-mol% MgO doping, Research Institute for Solid State Physics and Optics, Hungarian Academy of Sciences, Budapest) was used as THz emitter. The THz pulse energy was measured by means of a pyroelectric detector (Coherent-Molelectron, P4-42) with an active area of 2 mm in diameter. The detector calibration was cross-checked by measurements with a Golay cell (QMC Instruments, OAD-7). For the energy measurements, the THz output from the crystal was imaged into the detector by an aspherical bi-convex lens made from high-density polyethylene and optimized for 1:1 imaging. Characterization of the THz beam profile was performed with a pyroelectric array camera (Pyrocam III, Spiricon). By acquiring several profiles along the propagation direction, divergence of the THz beam was estimated.

The temporal THz field measurements were accomplished by means of electro-optical sampling [24] in a 100- μ m-thick <110> GaP crystal. The calibration of the balanced detector signal was performed by measuring the modulation signal induced by a calibrated weak absorber placed in front of each detector. The THz beam was focused into the crystal by a paraboloidal mirror with an effective focal length of 50 mm.

2.2. Simulation

The performance of different optical imaging schemes was estimated by ray tracing simulation using an in-house code. As the important spatial plane is that in which the pulse-front tilt is introduced (here the horizontal plane), we propagated a set of rays starting from a linear array of points passing through the vertical center of the input beam. As the orientation and position of all optical components were chosen so that no vertical deflection results for these rays, the simulation is effectively two-dimensional. For the simulation, three wavelengths within the bandwidth of the femtosecond pump pulse were chosen: the central wavelength and two side wavelengths that correspond to the FWHM points of the spectrum. Initially, all three pulse-fronts were chosen to be perpendicular to the direction of the beam propagation and to overlap in space, thus assuming zero chirp for the initial femtosecond pulse. After propagation over the grating and imaging optics, the pulse fronts for each wavelength were reconstructed inside the entry face of the LN crystal by calculating the group delay τ along each ray, i.e.

$$\tau = \frac{L}{c} \left(n - \lambda \frac{dn}{d\lambda} \right),$$

in a manner similar to that presented in ref [25]. The use of 5 rays across the beam was found to be yield sufficiently accurate results. Examples of reconstructed pulse fronts are shown in Fig. 1 for two imaging schemes consisting of a (a) single plano-convex lens and (b) a single concave mirror.

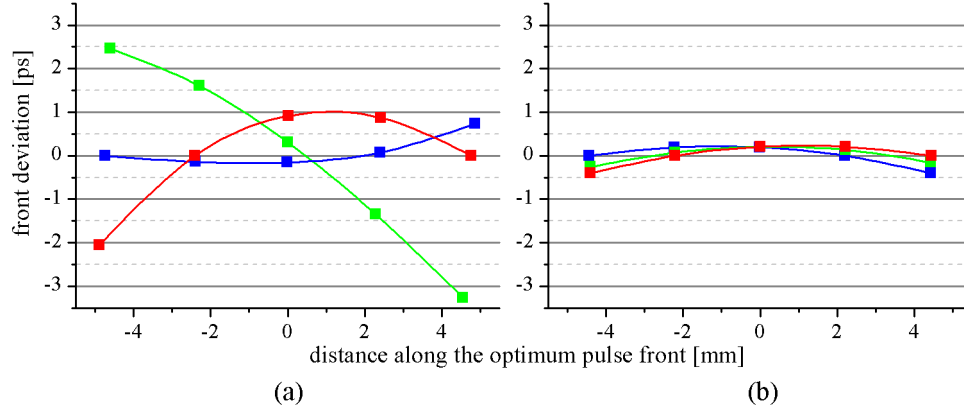


Fig. 1. Reconstructed pulse-fronts in the crystal for the optimized imaging geometries consisting of (a) a single plano-convex lens and (b) a single concave mirror (right). Blue, green and red correspond to 765, 780 and 795 nm, respectively. The line $Y = 0$ corresponds to the optimum pulse front with a tilt of 63° .

Here we define the group delay for each ray across the beam relative to the surface at 63° to the input face of the LN crystal, such that the zero corresponds to the optimal pulse front tilt for this center wavelength (assuming the phase (wave) front is parallel to the entry face). Next we introduce the following distortion parameter:

$$p = \sum_{i,j} \frac{\Delta t_{ij}}{NMd}.$$

Here Δt_{ij} is the absolute time deviation of the pulse-front point that corresponds to the i -ray and j -wavelength from the optimal 63° pulse front, N and M are the numbers of rays and wavelengths used in the simulation, respectively, and d is the average width of the beam in the crystal. The meaning of the parameter p can be easily understood by considering Fig. 1. This is an average deviation of all pulse front points from the optimum pulse-front tilt of 63° . If all pulse fronts acquire the optimum tilt, the parameter p is zero and the spatio-temporal distortions due to imaging are negligible. Thus, the better the imaging scheme, the smaller the distortion parameter p .

In order to compare the performance of different imaging geometries, the longitudinal positions and horizontal tilts of all optical elements (apart from the crystal, where the entrance surface was always chosen to be perpendicular to the middle ray of the central wavelength) were optimized by minimizing the distortion parameter p . For this purpose the Differential Evolution algorithm [26] was utilized, which is capable of localization of the global minimum for a multi-modal optimization problem. Note that the inclusion of the beam width d in the definition of p is required for such optimization (such that the average *angle* deviation of the pulse front is minimized), to prevent the tendency for the algorithm to converge on strongly focused beam.

3. Results and discussion

3.1 THz energy performance

The tilted-pulse-front pumping schemes that have been analyzed in the current work are shown in Fig. 2.

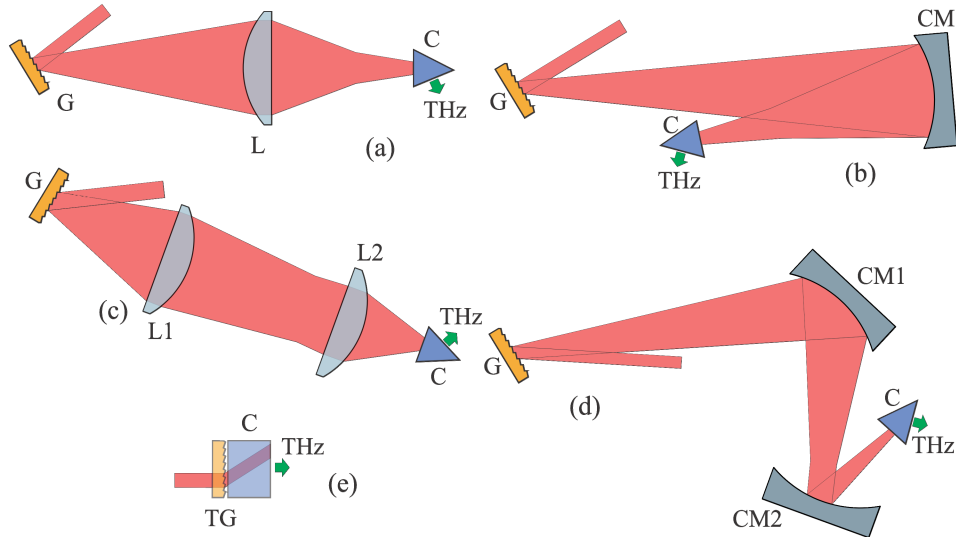


Fig. 2. The tilted-pulse-front pumping schemes for THz generation investigated in the current work. G – 2000 groves/mm grating, TG – transmission grating, C – LiNbO₃ crystal, L – lens, CM – spherical concave mirror. Focal lengths: $f(L) = 75$ mm, $f(L1, CM1) = 200$ mm, $f(L2, CM2, CM) = 100$ mm. Optimized geometries and other details are given in the supplementary file (Media 1).

The simulated and experimental performance of the different schemes is compared in Table 1. As one can see, the conventional imaging scheme with a single plano-convex lens (Fig. 2(a)) has the highest distortion parameter, especially with 35-fs pump pulses. The deviation of the pulse-fronts from optimum for this case is shown on Fig. 1(a). The initial femtosecond pulse is reconstructed at the center of the pump beam, while on the edges of the beam, the group-delay fronts are separated by a few ps due to imaging errors, resulting in a very long pulse length and very low peak intensity. Therefore the generation of the THz field is expected mainly around the central part of the pulse front, which leads to a rather low THz generation efficiency. This “point source” behavior of lens imaging was mentioned previously by Pálfalvi and associates [16]. Employment of a biconvex lens instead of the plano-convex lens results in a factor of 1.5 smaller distortion parameter p .

In order to increase the efficiency of THz generation, some groups [16,17] used an achromatic lens as an imaging element. This, however, according to our simulations (AC508-075-B from Thorlabs, $f = 75$ mm), brings about only two times smaller distortion parameter with respect to a single element plano-convex lens. One reason for this is the fact that an achromatic lens is usually designed for an infinite conjugation ratio operation, while in an imaging scheme usually a conjugation ratio of 2 is employed.

Further improvement of the imaging performance might be achieved by using a single mirror (Fig. 2(b)), which does not introduce any chromatic aberrations. The distortion parameter obtained from the ray-tracing simulation becomes five times smaller for broadband pump pulses compared to the single plano-convex lens imaging scheme (Fig. 1(a)). The experimental THz yield with the 35-fs 500- μ J pump pulses was measured to be 30 nJ, which is about three times better than that measured when using the single plano-convex lens scheme. Thus, the chromatic aberrations make up the main contribution to the pump pulse distortion in the case of broadband 35-fs pulses.

Table 1. Performance Comparison of Different Tilt-pulse-front Pumping Schemes^a for THz Generation in LN Crystal

Imaging scheme	35 fs, 30 nm@780 nm			150 fs, 9 nm@780 nm		
	p , fs·cm ⁻¹	demagnification ratio	exp. energy, nJ ^b	p , fs·cm ⁻¹	demagnification ratio	exp. energy, nJ ^a
plano-convex lens	984	2.1	9	225	2.2	59
biconvex lens	632	2.3	-	212	2.2	-
achromatic lens	593	1.8	-	200	2.2	-
concave mirror	199	2.0	30	157	2.1	-
lens telescope	40	1.6	-	16	1.6	-
mirror telescope	9	1.7	58	4	1.7	-
contact-grating	<5	-	-	<1	-	-

^aOnly “real” optical arrangements are considered, where rays and optical elements are not allowed to be overlapped with each other

^bPump energy of 0.5 mJ/pulse was used in experiments

A single mirror as an imaging element still introduces significant spherical aberrations. This contribution to the imaging errors should not be underestimated, especially when one considers that usually the whole aperture of the (50-mm diameter) mirror is illuminated by a broadband pump pulse after diffraction from the grating. The spherical aberrations could be partially compensated by utilizing two spherical mirrors in a Keplerian telescope arrangement (Fig. 2(d)). This allows one to decrease the distortion parameter by a factor of about 20 (relative to the single-mirror configuration), which experimentally resulted in an increase of the THz generation efficiency by about a factor of 2 compared to the single-mirror scheme. Experimentally, the 2-to-1 reflective Keplerian telescope brings about 6 times better THz performance than the conventional single plano-convex lens imaging if short 35-fs pump pulses are used.

Likewise, the imaging error of a single lens might be significantly minimized by using two lenses as a refractive Keplerian telescope (Fig. 2(c)). In this way the second lens partially compensates chromatic and spherical aberrations introduced by the first lens. A similar increase in THz generation efficiency, compared to a single-lens imaging scheme, was found by Palfali et al. [16] for a 1:1 relay-imaging telescope.

Palfalvi et al. [16] proposed a contact-grating scheme for tilting the pulse front of the pump (see Fig. 2(e)). This setup allows one to completely omit the imaging optics, and, thus, all kinds of aberrations they can cause. According to ray tracing simulations, an ideal contact-grating arrangement, where the crystal surface acts as a transmission grating, has an aberration parameter of better than 5 fs·cm⁻¹, which would correspond to the ultimate performance among the tilted pulse-front setups for THz generation in a LN crystal. However, the technical implementation of such a scheme is rather demanding. The main issue is the large refractive index of LN (2.26 at 780 nm), which makes it difficult to get the desired pulse-front tilt of 63° inside the crystal. The possible solution of this issue would be blazing/etching a grating directly on the crystal surface. Two designs of such a grating with diffraction efficiency above 90% have been recently proposed [27,28].

In contrast to the results and discussion above for the short pump pulses with a bandwidth of 30 nm, for the longer 150-fs pulses (with a 9-nm bandwidth) the distortion parameter is not significantly different for the imaging schemes consisting of a single lens or a single concave mirror, as chromatic aberrations do not play a significant role across such a relatively narrow bandwidth. However, as the pump pulses become shorter and their spectral bandwidth broader, chromatic aberrations become the dominant source of distortion (Fig. 3). Since telescope arrangements also allow for partial compensation of spherical aberrations, these arrangements bring about a significant distortion reduction even in the case of a narrow-bandwidth pump.

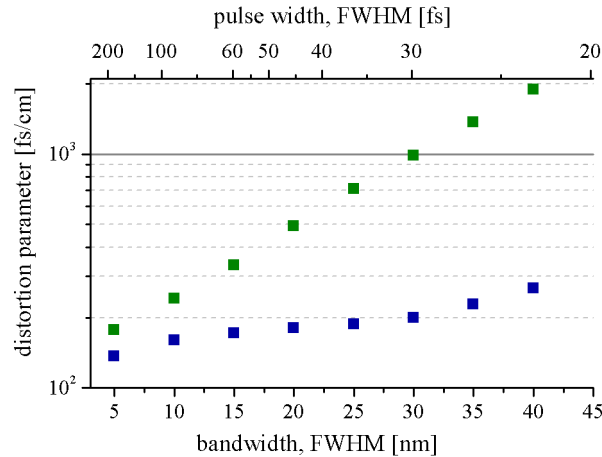


Fig. 3. Dependence of the distortion parameter p on the pump bandwidth for imaging schemes with a single lens (green) and a single concave mirror (blue). Note the logarithmic vertical scale. On the top axis the temporal width of the corresponding transform-limited pulse is given. The optical layout was optimized separately for each point in the graph.

It should be noted that while the dependence of the distortion parameter vs. pump bandwidth indeed reflects the effects of spatio-temporal imaging, it does not reflect quantitatively the absolute THz conversion efficiency since the peak intensity of the pump in the crystal (for a given pump pulse energy) also depends on the pulse duration.

The highest energy conversion efficiency achieved in the present paper (in terms of the THz beam after exiting the crystal) with the mirror telescope imaging for 35-fs 0.5 mJ pump pulses was $1.2 \cdot 10^{-4}$. This value is somewhat smaller than the average conversion efficiency of about $6 \cdot 10^{-4}$ reported in refs [15,29,30]. While the role of the pump pulse energy amongst these reports is difficult to address (due to the different degrees of efficiency saturation), one key reason for these higher conversion efficiencies is the use of longer optical pump pulses (85-400 fs). Utilization of even longer (1.3 ps) pump pulses [13] as well as narrowing of their spectral bandwidth [31] was also reported to achieve energy conversion efficiencies of about $2 \cdot 10^{-3}$. Stepanov et al. [18] reported conversion efficiency of $1 \cdot 10^{-3}$ by using 28-mJ 50-fs pump pulses and the imaging element consisting of a single concave mirror. In terms of sub-50-fs optical pump pulses, the highest performance reported to date [17] employed 25-fs 1.8-mJ pump pulses with a single achromatic lens for imaging into the crystal, with a measured THz pulse energy of 1.7 μ J. Based on our findings here, it is difficult to reconcile this high conversion efficiency ($\sim 10^{-3}$), and a direct experimental comparison of the THz pulse energy using spherical mirrors vs. an achromatic lens using the same experimental apparatus would be valuable to resolve this issue.

3.2. THz beam divergence

Not only the THz pulse energy, but also the divergence properties of the THz beam depends on the imaging scheme employed. This can have an important impact on the degree of focusability and resulting THz peak field. By performing raster line scans of the THz beam as a function of distance after the LN crystal, we characterized the beam profile and divergence in each lateral dimension. The results are shown in Fig. 4.

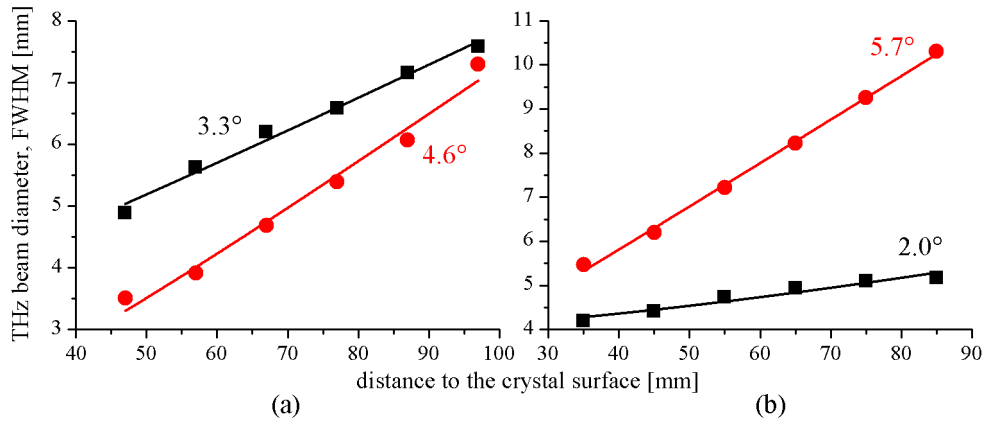


Fig. 4. THz beam divergence measured for imaging setups consisting of (a) a single mirror and (b) a mirror telescope (right). Black squares – in horizontal plane, red circles – in vertical plane. Solid lines are corresponding fits with Gaussian beam axial profiles assuming THz frequency of 1 THz.

A single concave mirror imaging results in a THz beam with a quite similar divergence in the horizontal (3.3°, FWHM) and vertical (4.6°, FWHM) planes (Fig. 4(a)). Tracing the linear fits back to the beam axis, the position of the virtual point source is seen to be significantly different for these two planes, which makes it impossible to use only one spherical focusing element for THz beam collimation. Instead two cylindrical lenses with different focal lengths may be used. The virtual point sources for horizontal and vertical planes are also displaced when a concave-mirror telescope is used for imaging. In this case the horizontal divergence (2.0°, FWHM) of the THz beam was found to be much smaller than the vertical one (5.7°, FWHM) (Fig. 4(b)). One can expect that the vertical divergence can be essentially minimized by employing cylindrical mirrors in the optical pump imaging telescope instead of spherical ones (Fig. 2(d)). The use of cylindrical imaging optics has already been demonstrated for longer optical pump pulses with two cylindrical lenses [30], resulting in a THz beam with a vertical divergence of 0.3°. For many applications a divergence of 2° may be appropriate, that no further collimation means will be necessary.

3.3. Field measurements

The measured temporal profile and the corresponding frequency spectrum of the THz radiation for the mirror telescope imaging setup are shown in Fig. 5. For this measurement, the THz beam was initially collimated in the vertical plane by a cylindrical lens made from high-density polyethylene with a focal length of 140 mm. Subsequently, the THz beam of about 16 mm (FWHM) in diameter was focused into a GaP crystal by means of a parabolic mirror with an effective focal length of 50 mm. Taking these parameters and using Gaussian beam approximation we have theoretically estimated the field strength of about 80 kV/cm for a 58-nJ 1-ps single-cycle THz pulse. This theoretical value is in a very good agreement with an experimental value of 60 kV/cm, taking in to account the reflection losses on the surfaces of the collimating lens and the GaP crystal.

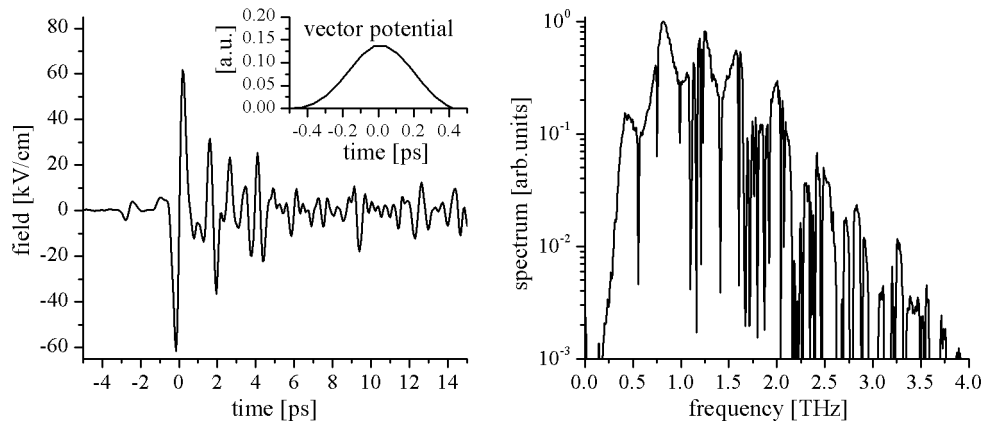


Fig. 5. The temporal profile and the corresponding frequency spectrum of THz radiation for the mirror-telescope imaging setup. As an inset the vector potential of the THz field around time-zero is presented. The vector potential is given in atomic units (1 a.u. = 124.4 kV-ps/cm).

One of the applications of THz pulses is streaking photoelectrons, which, for instance, may be used for characterization of ultrashort (much shorter than a single cycle of the THz field) laser pulses [32,33]. In these pump-probe experiments a photoelectron is ejected by a VUV photon pulse e.g. from a free electron laser. The VUV pulse is overlapped with the THz pulse and hence the photoelectron is accelerated (or decelerated) by the THz field depending on the time it was born with respect to the THz field. In this way the time instance of ionization can be mapped onto freed electron momentum space. The time resolution is determined by the derivative of the vector potential of the streaking field. In the inset of Fig. 5 the vector potential of the THz field around time-zero is shown. The highest derivative of vector potential at times ± 0.2 ps corresponds to a momentum change of 0.46 a.u. per picosecond, which would be measured on a photoelectron in a pump-probe experiment.

4. Conclusions

In the present work different imaging schemes for tilted-pulse-front pumping THz generation in the LiNbO₃ crystal have been analyzed. It has been shown that chromatic and spherical aberrations introduced by an imaging element can significantly reduce the energy performance of THz generation in the case of broadband pump pulses with duration shorter than 50 fs. The ray tracing simulation code has been developed and applied for optimizing and comparing aberrations of different imaging schemes. The conventional single-lens imaging scheme was found to be highly inefficient for broadband ultra-short pump pulses, mainly due to chromatic aberrations. The best performing imaging scheme has been found to consist of two concave mirrors in a Keplerian telescope arrangement. This setup is free of chromatic aberrations, while spherical aberrations are partially compensated because of the use of two spherical elements in series. The experimental energy conversion efficiency for this scheme was found to be 6 times better than that of a conventional single-lens imaging for our laser system with 35-fs pump pulses. For longer pump pulses with narrower bandwidth chromatic aberrations of the imaging scheme is not a main concern. However, even for longer pulses, the employment of two spherical optical elements in series for imaging is justified, since it results in a significant reduction of spherical aberrations.

The omission of imaging optics in the contact-grating scheme proposed by Hebling and associates [16] would allow one to avoid such aberrations completely. The technical implementation of this setup is however rather challenging because of the large refractive index of the LiNbO₃ crystal and significant pulse-front tilt required for 800 nm pump pulses. Blazing/etching a grating directly on the crystal surface would allow to overcome the issue,

bringing about the ultimate performance among tilted-pulse-front pumping setups for THz generation in LiNbO₃ crystal.

Acknowledgments

The financial support of the Goethe-University Frankfurt am Main is gratefully acknowledged.